Active Disturbance Rejection Control of a Magnetic Screw Motor for High Tracking Performance

Guohai Liu, *Senior Member, IEEE*, Lixian Fang, Zhengmeng Liu, Qian Chen, *Senior Member, IEEE*, and Jiahao Zhang

***Abstract*—A magnetic screw motor integrated by a magnetic screw and a permanent magnet synchronous motor offers high thrust density without friction and loss. However, its internal structure is complicated, resulting in difficulty to control its linear displacement to track the given signal in time and even getting out of control due to interference. In this article, to improve the tracking performance and anti-interference performance of the system, an active disturbance rejection controller (ADRC) is adopted to improve the current loop and makes up for nonlinear regional control in the closed-loop control system. To ensure the stability of the proposed scheme in the entire operation range, the design and the stability analysis are carried out in the continuous-time domain. The novel control algorithm enhances the flexibility of the magnetic screw motor by optimizing the nonlinear function in ADRC. In addition, to highlight the high-performance control of the ADRC for the magnetic screw motor, sliding mode control and PI control are added to compare with it. Finally, the reciprocating motion control is added to show the diversity of the functions of the magnetic screw motor, which verifies the effectiveness and feasibility of the control algorithm.**

***Index Terms*—Active disturbance rejection controller (ADRC), displacement control, magnetic screw motor, sliding mode control (SMC), traditional PI controller.**

I. Introduction

With the increase of the complexity of the drive system and the improvement of the drive accuracy requirements, the linear and rotational driving characteristics have received extensive attention [1]–[3]. As a power transmission part connecting the vehicle body with the axle or wheel, the requirements of active suspension for high-performance linear actuator have increased sharply. In recent years, various high-performance linear actuators emerge in an endless stream, such as electrohydraulic linear actuators [4], [5], electromechanical linear actuators [6], [7], and direct-driveelectric linear actuators [8]. In most of the current research fields of linear actuators, permanent magnet linear actuators are widely praised with its high thrust density and high efficiency [9]–[11]. Until now, research on linear magnetic screw actuators has begun to emerge [12], [13]. Compared with traditional mechanical screws, these magnetic screws have the advantages of high force density and inherent overload protection. At the same time, through the contactless force transmission of the magnetic field, they have almost no friction in the process of movement.

Recently, a high-force-density linear actuator has been developed and applied to vehicle suspension [14], [15]. In this article, the magnetic screw motor researched is obtained by integrating the abovementioned magnetic screw and permanent magnet synchronous motor (PMSM). The motor pushes the magnetic screw forward through the action of rotating magnetic field with almost no friction and loss. With its special internal structure, it can output a force of about 5 kN at most. However, due to the complexity and uncertainty of the magnetic screw motor involved in this article, it greatly increases the difficulty of control.

Nowadays, a variety of magnetic screws with different structures and different properties [16]–[19] are being researched. As a result, it has a broad application prospects in the field of linear motion. However, the research on the control strategy of the magnetic screw is not yet mature. In [20], a high thrust direct drive linear actuator with a helical structure is designed. The permanent magnet motor has a wide gap area on the three-dimensional structure and has high thrust characteristics. Then, decoupling control is proposed and disturbance observer is adopted to improve the robustness of the system. Finally, the problems of safety and high performance in robot application are successfully solved. Similar to the former motor, the mover of the motor in [21] hardly contacts the stator and moves spirally in a wide gap. The magnetic conductivity method is adopted to calculate the thrust and torque equation, as well as the experiment shows that the thrust reaches 2 kN. In [22], the internal structure of a helical motor with a single joint structure is equipped with a needle tube shape to generate sufficient current to perform driving. Similarly, decoupling and independent control are still adopted to realize synchronous angular motion control. In [23], a control method of energy-saving axial clearance displacement adjustment is proposed for a screw motor. Since the balance point between the magnetic field of the mover and the electron

Manuscript received January 7, 2022; accepted March 11, 2022. Date of publication March 23, 2022; date of current version April 28, 2022. This work was supported in part by the National Natural Science Foundation of China under Grant 51877098 and Grant 52077097, in part by the Natural Science Research Project of Higher Education Institutions of Jiangsu Province under Grant 20KJA470003, in part by China Postdoctoral Science Foundation under Grant 2021M701647, and in part by the Priority Academic Program Development of Jiangsu Higher Education Institutions. Recommended for publication by Associate Editor N. R. Idris. *(Corresponding author: Zhengmeng Liu.)*

Guohai Liu, Lixian Fang, Zhengmeng Liu, Qian Chen, and Jiahao Zhang are with the School of Electrical and Information Engineering, Jiangsu University, Zhenjiang 212013, China, and also with the Jiangsu Key Laboratory of Drive and Intelligent Control for Electric Vehicle, Jiangsu University, Zhenjiang 212013, China (e-mail: ghliu@ujs.edu.cn; 2222007005@stmail.ujs.edu.cn; lzm@ujs.edu.cn; chenqian0501@ujs.edu.cn; 2112107015@stmail.ujs.edu.cn).

Color versions of one or more figures in this article are available at https://doi.org/10.1109/TPEL.2022.3161353.

Digital Object Identifier 10.1109/TPEL.2022.3161353

is not easy to determine, the method reduces the copper loss by controlling the relative displacement. In [24], a radial gap helical machine in which the surfaces of the mover and the rotor are pasted with spiral layered permanent magnet is proposed. Cascade control of proportional and disturbance observers is adopted to control linear position and angular velocity simultaneously. However, the existing control strategies for the magnetic screw motor lack consideration of the nonlinear region, which will lead to the deterioration of the current loop due to the uncertainty of the magnetic field force. In other words, traditional direct drive control cannot meet the requirements of dynamic performance and robustness of high-performance magnetic screw motor system. Hence, the effective control strategies must be adopted to weaken the impact of disturbances on the system performance.

With the advantages of strong anti-interference ability, high tracking accuracy, and fast response speed, ADRC effectively solves many problems of the control strategy. In [25], a combined control strategy of vector resonant and ADRC is proposed, which can suppress the current harmonics and improve the current waveform and output thrust. However, this algorithm ignores the design of the tracking performance of the system and cannot be applied into the magnetic screw motor directly. In [26], a hybrid position estimation strategy combining the electromotive force estimation in the high-speed region and high-frequency current injection in the low-speed region is proposed to reduce the phase delay and speed jitter. Although the first-order ADRC is suitable for the magnetic screw motor, the design of nonlinear function is not considered, which will affect the subsequent experimental results directly. In [27], ADRC is adopted to compensate for the displacement error caused by disturbance. If the second-order ADRC is directly applied to the position loop, the control process will become more complicated, which will increase the control difficulty of magnetic screw motor. How to effectively match the structure and performance of ADRC and magnetic screw motor has become the main breakthrough point in the current work.

Due to the complex internal structure of magnetic screw motor, the difficulty of its control is to eliminate the interference of magnetic field force when controlling linear and rotating parts at the same time. In this article, ADRC is adopted to improve the current loop and makes up for nonlinear regional control in the closed-loop control system. The main contributions of this article are listed as follows.

1) The mathematical model of magnetic screw motor is established by connecting the rotating part with the linear part. According to the internal structure of the magnetic screw, it is determined that the main interference comes from the instability of the magnetic force, which results in the deterioration of the current loop. Moreover, the relationship between current and magnetic field force is derived.
2) Aiming at the problem of magnetic field force interference, ADRC is introduced to make up for the lack of nonlinear regional control in the closed-loop control system. The disturbance of the current loop uncertainty of the magnetic screw motor is compensated, which improves the stability and dynamic performance of the control system.
3) The difference fitting method is adopted to smooth the nonlinear function in the core NLSEF of ADRC, which strengthens the high tracking performance of input signal and the flexibility of magnetic screw operation. In addition, the feasibility of the control algorithm is proved by the stability analysis of the novel ADRC. SMC [28] and PI control are added and compared with ADRC to highlight its high-performance control. To prove the robustness and anti-interference of ADRC, experiments on the inductance parameter mismatch are carried out in this article.

This article is divided into five sections. In Section II, the block diagram and introduction of the entire model of the internal structure of the magnetic screw motor are included. The mathematical model of the magnetic screw motor and the design of ADRC based on the current loop are described in Section III. In Section IV, the experiments are accomplished to demonstrate the control strategy of this paper. Finally, Section V concludes this article.

II. Motor Description

Fig. 1(a) shows the cross-sectional view of the magnetic screw motor researched in this article. It is essentially a linear actuator with high thrust density, including an 18-slot, 8-pole permanent magnet rotating motor and a magnetic screw. The rotor is located between the stator and the mover and radial permanent magnets are helically attached to the air gap between the rotor and the stator. In order to achieve a thrust density equivalent to that of a mechanical gear drive system, a drive topology that integrates a magnetic screw into a permanent magnet motor is adopted. Fig. 1(b) presents the cross-sectional view of the magnetic screw and the magnetic screw and PMSM share the same rotor. The rotor is located on the outer layer while the mover is located on the inner layer. Two spiral permanent magnet arrays with opposite magnetization directions distributed on the inner surface between the mover and the stator. Since the magnetic screw itself has no windings, the rotor needs external input to achieve rotation. When the rotor rotates, the torque will be transmitted to the mover through a gear transmission similar to a mechanical ball screw. If one end of the mover is fixed at this time, the mover will perform linear motion to generate thrust output.

Fig. 1(c) describes the internal structure of the magnetic screw, where ω and T are the rotor angular velocity and torque respectively; γ is the pole pitch of the permanent magnet; λ is the lead of the magnetic screw; v and F_t are the linear velocity and thrust of the mover, respectively. There is a very small air gap between the pair of permanent magnets, and the distance of this air gap is far less than the pole pitch of the permanent magnets. Therefore, the relationship between the lead and the pole pitch can be approximately regarded as a double relationship: $\lambda = 2\gamma$.

In general, the magnetic screw motor completes the transmission of mechanical energy but has not changed the form of energy. Besides, this mechanical energy transfer is completed by the magnetic coupling force rather than the previous mechanical contact between the mover and the rotor. The electromagnetic force is generated by the interaction between the rotor's magnetic field and the mover's magnetic field. Since the mover is bolted

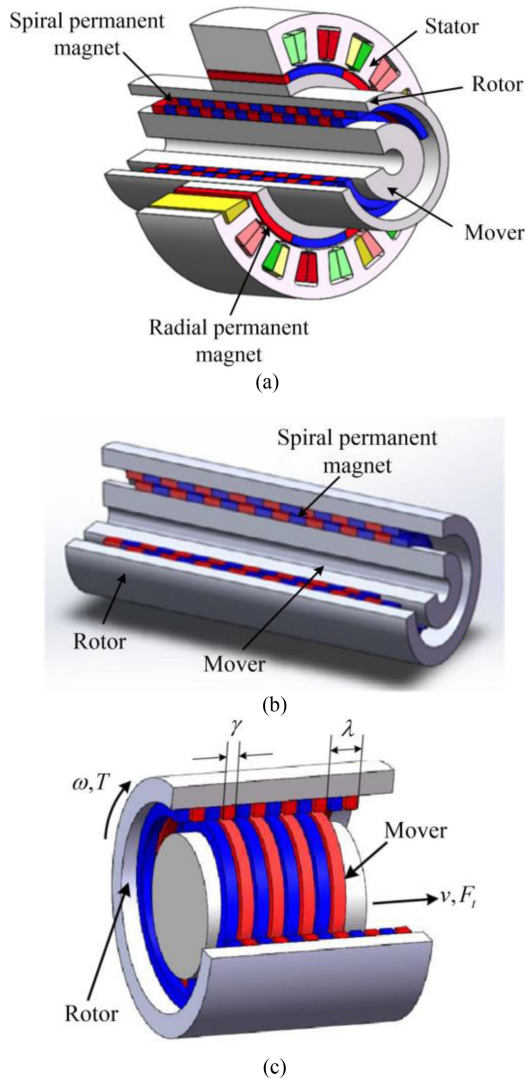

Fig. 1. Three-dimensional schematic of the magnetic screw motor. (a) Integrated actuator. (b) Magnetic screw. (c) Internal structure of magnetic screw.

when realizing the control of linear displacement, this structure will vibrate violently and move forward. However, under the optimization of active disturbance rejection, this structure greatly reduces the jitter. Therefore, the linear displacement can be controlled quickly and smoothly.

III. Mathematical Model

A. Model of Permanent Magnet Synchronous Motor

The magnetic screw motor in this article is integrated by a three-phase PMSM and a magnetic screw.

In the three-phase static coordinate, the voltage equation of the stator can be expressed as

$$\begin{bmatrix} u_a \\ u_b \\ u_c \end{bmatrix} = \begin{bmatrix} R_s & 0 & 0 \\ 0 & R_s & 0 \\ 0 & 0 & R_s \end{bmatrix} \begin{bmatrix} i_a \\ i_b \\ i_c \end{bmatrix} + \begin{bmatrix} \dot{\psi}_a \\ \dot{\psi}_b \\ \dot{\psi}_c \end{bmatrix} \tag{1}$$

where u_a, u_b, and u_c are the three-phase voltages of the stator; i_a, i_b, and i_c are the three-phase currents of the stator; ψ_a, ψ_b, and ψ_c are the three-phase winding flux linkages; R_s is the stator resistance.

The flux equation of the stator can be given by

$$\begin{bmatrix} \psi_a \\ \psi_b \\ \psi_c \end{bmatrix} = \begin{bmatrix} L_{aa} & M_{ab} & M_{ac} \\ M_{ba} & L_{bb} & M_{bc} \\ M_{ca} & M_{cb} & L_{cc} \end{bmatrix} \begin{bmatrix} i_a \\ i_b \\ i_c \end{bmatrix} + \begin{bmatrix} \psi_{fa} \\ \psi_{fb} \\ \psi_{fc} \end{bmatrix} \tag{2}$$

where L_{aa}, L_{bb}, L_{cc} are the self-inductance of the stator, respectively; $M_{ab}, M_{ac}, M_{ba}, M_{bc}, M_{ca}, M_{cb}$ are the mutual inductance of the stator, respectively; ψ_{fa}, ψ_{fb}, and ψ_{fc} are the flux linkages of the stator windings produced by the permanent magnets, which can be expressed as

$$\begin{bmatrix} \psi_{fa} \\ \psi_{fb} \\ \psi_{fc} \end{bmatrix} = \psi_f \begin{bmatrix} \cos\theta \\ \cos(\theta - 120^\circ) \\ \cos(\theta + 120^\circ) \end{bmatrix}. \tag{3}$$

After Park transformation, the voltage equation of the stator in the synchronous rotating coordinate system can be obtained as

$$\begin{bmatrix} u_d \\ u_q \end{bmatrix} = R_s \begin{bmatrix} i_d \\ i_q \end{bmatrix} + \begin{bmatrix} \dot{\psi}_d \\ \dot{\psi}_q \end{bmatrix} + \begin{bmatrix} -\omega\psi_q \\ \omega\psi_d \end{bmatrix} \tag{4}$$

where $u_{d,q}$ and $i_{d,q}$ are stator voltage and current in *dq*-axes, respectively; ψ_d and ψ_q are *dq*-axes stator winding flux linkages; ω is the electrical angular velocity of the rotor.

In the synchronous rotating coordinate system, the stator flux equation can be obtained as

$$\begin{bmatrix} \psi_d \\ \psi_q \end{bmatrix} = \begin{bmatrix} L_d & 0 \\ 0 & L_q \end{bmatrix} \begin{bmatrix} i_d \\ i_q \end{bmatrix} + \begin{bmatrix} \psi_f \\ 0 \end{bmatrix} \tag{5}$$

where L_d and L_q are the inductances of the *dq*-axes, respectively. By substituting (5) into (4), the voltage equation can be elaborated as

$$\begin{bmatrix} \dot{i}_d \\ \dot{i}_q \end{bmatrix} = \begin{bmatrix} -\frac{R_s}{L_d} & \frac{\omega L_q}{L_d} \\ -\frac{\omega L_d}{L_q} & -\frac{R_s}{L_q} \end{bmatrix} \begin{bmatrix} i_d \\ i_q \end{bmatrix} + \begin{bmatrix} \frac{1}{L_d} & 0 \\ 0 & \frac{1}{L_q} \end{bmatrix} \begin{bmatrix} u_d \\ u_q \end{bmatrix} - \begin{bmatrix} 0 \\ -\frac{\omega\psi_f}{L_q} \end{bmatrix}. \tag{6}$$

The equations of motion for the rotational position of the rotor and the linear displacement of the mover can be obtained as

$$\begin{cases} J\ddot{\theta}_m = p\psi_f i_q + (L_q - L_q) i_d i_q + T_m \\ M\ddot{x} = f_m - f_l \end{cases} \tag{7}$$

where M is the mass of the mover; J is the moment of inertia; θ_m is the mechanical rotation angle; T_m is to overcome the torque of rotor; f_m is the electromagnetic thrust generated between permanent magnets; f_l is the external load force.

B. Model of the Magnetic Screw

The researched permanent magnet motor is a surface mount type: $L_d = L_q$. When the load force exceeds a certain limit, the displacement between permanent magnets exceeds 1/4λ, which causes the motor movement out of control. In addition, if the relative displacement x_d is close to 0, the electromagnetic

thrust f_m is proportional to x_d, i.e., when x_d<1/4λ, the following equation can be obtained as

$$f_m = -Q_m x_d \tag{8}$$

where Q_m is the coefficient of rotation; $x_d = x+h\theta$ is the relative displacement between the permanent magnet and the mover, x is the axial displacement of the mover; parameter $h = \lambda/2\pi$; θ is the electrical angle.

The relationship between the rotor angular velocity ω and the linear velocity v of the mover can be obtained as

$$\omega = 2\pi\frac{v}{\lambda}. \tag{9}$$

The transmission of mechanical energy comes from the interaction of the magnetic field between the mover and the rotor. According to the law of conservation of energy, (10) needs to be satisfied

$$\dot{\theta}_m \tau_s + \dot{x} f_s = 0. \tag{10}$$

The thrust from the mover is approximately related to the torque to overcome the rotor, which can be expressed as

$$T_m = \frac{\lambda}{2\pi} f_m. \tag{11}$$

When the magnetic screw completes the linear movement, the motor will be in a balanced state. However, at this time, the magnetic pole position between the mover and the rotor cannot be figured out. Combining (7) and (11), the relationship formula between current and electromagnetic thrust can be expressed as

$$i_q = -\frac{\lambda}{2\pi p \psi_f} f_m. \tag{12}$$

C. PI Control, SMC, and ADRC

PI control, as a kind of traditional motor vector control, adopts weighted summation method to make the deviation between the desired target and the actual behavior close to zero. Unfortunately, PI control cannot solve the contradiction between the rapidity of the system and the overshoot, which often leads to problems in the performance of the control system. Sliding mode control makes the system run according to the law specified by sliding mode through switching function. However, the discontinuity of control leads to the inevitability of chattering. System and control expert Prof. J. Han adopted special nonlinear effects to develop links with special functions, thus forming the active disturbance rejection controller.

D. Model of ADRC

ADRC is divided into three parts: tracking differentiator (TD), nonlinear state error feedback (NLSEF), and extended state observer (ESO). TD arranges a reasonable transition process for the input signal and can effectively reduce the overshoot and error. Besides, NLSEF controls and compensates the errors of input signal and its differential signal, as well as output signal and its derivative, which can reflect the total disturbance of the system in real time and feed back to the front tracking signal.

According to the control requirements of engineering, the object can be controlled efficiently by assigning appropriate parameters and nonlinear functions to ADRC. The control formula can be expressed as follows:

$$\begin{cases} x^{(n)} = f(x, x', \ldots x^{(n-1)}, t) + q(t) + bu \\ y = x(t) \end{cases} \tag{13}$$

where $f(x, x', x^{(n-1)}, t)$ is the unknown function; $x(t)$ is the state of the system; $q(t)$ is the unknown disturbance affecting the system; u is the input signal after control; b is the gain of the control quantity; y is the output of the system.

N-order TD can be expressed as

$$\begin{cases} z_{11}{}' = z_{12} \\ z_{12}{}' = z_{13} \\ \vdots \\ z_{1n}{}' = z^n f(z_{11} - v(t), \frac{z_{12}}{E}, \ldots, \frac{z_{1n}}{E^{n-1}}) \end{cases} \tag{14}$$

where z_{11} is the tracking signal of the input signal $v(t)$; E is the limit of $v(t)$; z_{11}' … z_{1n}' is the differential signal of each order of $v(t)$.

(N+1)-order TD can be expressed as

$$\begin{cases} z_{21}{}' = z_{22} - h(z_{21} - x(t)) \\ \vdots \\ z_{2n}{}' = z_{2n+1} - h_n(z_{21} - x(t)) + bu \\ z_{2n+1}{}' = -h_{n+1}(z_{21} - x(t)) \end{cases} \tag{15}$$

where z_{21} is the tracking signal of the output signal $y(t)$; z_{21}' … z_{2n}' is the differential signal of each order of $y(t)$; z_{2n+1}' is the observation value of the total disturbance $w(t)$, which can be given by

$$w(t) = f(x, x', \ldots x^{(n-1)}, t) + q(t). \tag{16}$$

When the controlled input signal is $u(t) = u_0(t)$-$w(t)/b$, the unknown disturbance can be estimated and compensated by $w(t)$.

In order to achieve the ideal control effect, NLSEF adopts $u_0(t)$ to modulate the N-order integrator series system, which can be expressed as

$$\begin{aligned} u_0(t) = {} & k_1 \text{fal}(\varepsilon_1, \alpha, \delta) \\ & + k_2 \text{fal}(\varepsilon_2, \alpha, \delta) + \ldots + k_n \text{fal}(\varepsilon_n, \alpha, \delta). \end{aligned} \tag{17}$$

The formula of nonlinear function fal(ε,α,δ) can be expressed as follows:

$$\text{fal}(\varepsilon, a, \delta) = \begin{cases} |\varepsilon|^a \text{sign}(\varepsilon) & |\varepsilon| > \delta \\ \varepsilon/\delta^{1-a} & |\varepsilon| \le \delta \end{cases} \tag{18}$$

where α is the nonlinear factor; δ is the error accuracy; ε is the tracking error of the system; k is the gain factor. Although the traditional nonlinear function fal(ε,α,δ) is continuous in all intervals, it is obviously not smooth and differentiable at the segment point of $\pm\varepsilon$. The mutation of numerical value often leads to the oscillation and overshoot of the output of the system. Therefore, a new nonlinear function fax(ε,α,δ) is constructed to improve the performance in this article.

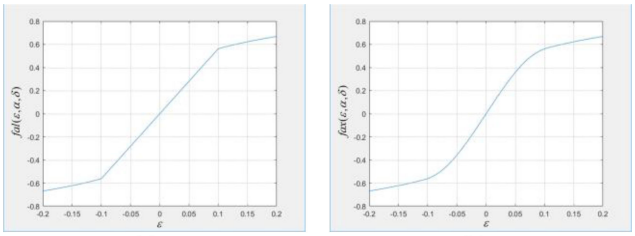

Fig. 2. Simulation images of the nonlinear functions. (a) fal(ε,α,δ). (b) fax(ε,α,δ).

The original power function is retained and the first-order function is replaced by interpolation fitting polynomial

$$\text{fax}(\varepsilon, \alpha, \delta) = p_1 x + p_2 x^2 + p_3 \sin x. \tag{19}$$

To fit the nonlinear function fal(ε,α,δ) with the nonlinear function fax(ε,α,δ), the piecewise points need to meet the following smooth and continuous conditions:

$$\begin{cases} \text{fax}(\delta, \alpha, \delta) = \delta^\alpha \\ \text{fax}(-\delta, \alpha, \delta) = -\delta^\alpha \\ \text{fax}(\delta, \alpha, \delta)' = a\delta^\alpha \\ \text{fax}(-\delta, \alpha, \delta)' = -a\delta^\alpha \\ \text{fax}(0, \alpha, \delta) = 0 \end{cases}. \tag{20}$$

Then, we can get the values of p_1, p_2, and p_3. The new nonlinear function can be expressed as

$$\text{fax}(\varepsilon, \alpha, \delta) = \begin{cases} |\varepsilon|^\alpha \text{sign}(\varepsilon) & |\varepsilon| > \delta \\ (\alpha\delta^{\alpha-1} + \frac{(\alpha-1)\delta^\alpha \cos\delta}{\sin\delta - \delta\cos\delta})\varepsilon - \frac{(\alpha-1)\delta^\alpha}{\sin\delta - \delta\cos\delta}\sin\varepsilon & |\varepsilon| \le \delta \end{cases} \tag{21}$$

The value of the nonlinear factor α in the power function generally ranges from 0 to 1. The error accuracy δ determines the linear interval degree of the function and has an impact on the deviation range of the system. Then, we assign a value of 0.1 here.

As shown in the Fig. 2, compared with the traditional nonlinear function fal(ε,α,δ), the new nonlinear function *fax*(ε,α,δ) can remain smooth and continuous in the entire interval. When the dynamic model of the controlled object cannot be determined accurately, this strategy can effectively suppress the steady-state error and reduce the error decay time.

E. Design of ADRC Based on the Current Loop

During the operation of the motor, the current loop plays an important role in the control of the three-phase PMSM. Compared with the PI controller, ADRC designs the transition process to make the input signal smoother and solves the contradiction between the overshoot and the rapidity. In addition, the nonlinear function is introduced to make up for shortcomings of the PI controller. Finally, ADRC adopts the ESO to effectively estimate the total disturbance of the motor and perform dynamic compensation in real time.

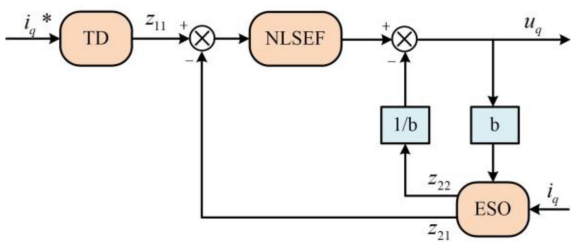

Fig. 3. Block diagram of ADRC in the *q*-axis current loop.

When the vector control strategy with $i_d = 0$ is adopted, (6) can be transformed into

$$\begin{cases} \dot{i}_d = \frac{1}{L_d}(-R_s i_d + \omega L_d i_q) + \frac{1}{L_d}u_d \\ \dot{i}_q = -\frac{1}{L_q}(R_s i_q + \omega\psi_f + \omega L_d i_d) + \frac{1}{L_q}u_q. \end{cases} \tag{22}$$

The control of the current will be affected by the resistance, inductance, and flux linkage. The disturbance to the *dq*-axes can be given by

$$\begin{cases} s_d(t) = \frac{1}{L_d}(-R_s i_d + \omega L_d i_q) \\ s_q(t) = -\frac{1}{L_q}(R_s i_q + \omega\psi_f + \omega L_d i_d). \end{cases} \tag{23}$$

Set b_d and b_q as the control gain coefficients, respectively. Combining (22) and (23), the first-order equation of the current loop can be obtained as

$$\begin{cases} \dot{i}_d = s_d(t) + b_d u_d \\ \dot{i}_q = s_q(t) + b_q u_q \end{cases}. \tag{24}$$

Therefore, a first-order ADRC for the *dq*-axes current loop can be constructed, which can be seen in Fig. 3. where i_q* is the ideal input signal of the current loop control system; z_{11} is used to track the input signal i_q*; the signal z_{21} in the ESO is used to observe the i_q current in real time; the signal z_{22} is used to observe the disturbance of the system; *b* is the control coefficient estimated by the model, which may deviate from the actual value due to machine aging and other problems.

Since ADRC of the *d*-axis eliminates the transition process, the tracking differentiator design can be cancelled. Then, taking the *q*-axis current loop as an example, the three-part mathematical model of the ADRC will be introduced.

The model of the TD can be obtained as

$$\begin{cases} \varepsilon_0 = z_{11} - i_q* \\ \dot{z}_{11} = -g_0 fax(\varepsilon_0, \alpha, \delta) \end{cases}. \tag{25}$$

The model of the ESO can be obtained as

$$\begin{cases} \varepsilon_1 = z_{21} - i_q \\ \dot{z}_{21} = z_{22} - g_{21}\text{fax}(\varepsilon_1, \alpha, \delta) + bu \\ \dot{z}_{22} = -g_{22}\text{fax}(\varepsilon_1, \alpha, \delta) \end{cases}. \tag{26}$$

The model of the NLSEF can be obtained as

$$\begin{cases} \varepsilon_2 = z_{11} - z_{21} \\ u_0 = g_3\text{fax}(\varepsilon_2, \alpha, \delta) \\ u = u_0 - z_{22}/b \end{cases} \tag{27}$$

where the tracking speed g_0 factor has an impact on the tracking effect of the signal. If the value is too large, overshoot and noise

will be generated; parameters g_{21} and g_{22} will affect the tracking speed of the system. Generally g_{22} is greater than g_{21}.

F. Stability Analysis of ADRC

Firstly, it is assumed that the magnetic screw motor is a linear constant system

$$\begin{cases} x^{(n)} = a_n x + a_{n-1}\dot{x} + \cdots + a_1 x^{(n-1)} + bu \\ y = x \end{cases}. \tag{28}$$

Set the input signal of the system to 0 and the output signal of TD to 0. The NLSEF is replaced by the linear state error feedback. The control law is as follows

$$u = \frac{u_0 - z_{n+1}}{b} = \frac{-\sum_n^{i=1} k_i z_i - z_{n+1}}{b}. \tag{29}$$

Set the nonlinear function as $g(x)$, which satisfies the condition: $xg(x)>0$, $x\neq 0$. The ESO can be expressed as

$$\begin{cases} e = z_1 - y \\ \dot{z}_1 = z_2 - \beta_1 g(e) \\ \vdots \\ \dot{z}_n = z_{n+1} - \beta_n g(e) + bu \\ \dot{z}_{n+1} = -\beta_{n+1} g(e) \end{cases}. \tag{30}$$

Combining (29) and (30), we can get the following expression:

$$\begin{cases} \dot{\mathbf{z}} = A_{22}\mathbf{z} + \mathbf{t}r \\ \dot{z}_{n+1} = \beta_{n+1} r \end{cases} \tag{31}$$

where $g(e) = -r$, $\boldsymbol{t} = [\beta_1, \beta_2, \ldots, \beta_n]^T$, $\boldsymbol{z} = [z_1, z_2, \ldots, z_n]^T$

$$A_{22} = \begin{bmatrix} 0 & 1 & 0 & 0 & \cdots & 0 \\ 0 & 0 & 1 & 0 & \cdots & \vdots \\ \vdots & \vdots & 0 & \cdots & \cdots & 0 \\ 0 & 0 & \cdots & \cdots & \cdots & 1 \\ -k_1 & -k_2 & \cdots & \cdots & \cdots & -k_n \end{bmatrix}.$$

The state-space expression of linear time invariant system can be expressed as

$$\begin{cases} \dot{\mathbf{x}} = A_{11}\mathbf{x} + A_{12}\mathbf{z} + \mathbf{J}z_{n+1} \\ y = x_1 \end{cases} \tag{32}$$

where $\boldsymbol{x} = [x_1, x_2, \ldots, x_n]^T$,, $\boldsymbol{J} = [0, 0, \ldots, -1]^T$

$$A_{11} = \begin{bmatrix} 0 & 1 & 0 & \cdots & \cdots & 0 \\ 0 & 0 & 1 & 0 & \cdots & 0 \\ 0 & \vdots & 0 & \cdots & \cdots & \vdots \\ \vdots & \vdots & \vdots & \vdots & \vdots & 0 \\ 0 & 0 & 0 & 0 & 0 & 1 \\ a_n & a_{n-1} & \cdots & \cdots & \cdots & a_1 \end{bmatrix}$$

$$A_{12} = \begin{bmatrix} 0 & \cdots & \cdots & \cdots & \cdots & 0 \\ \vdots & & & & & \vdots \\ \vdots & & & & & \vdots \\ 0 & \cdots & \cdots & \cdots & \cdots & 0 \\ -k_1 & -k_2 & \cdots & \cdots & \cdots & -k_n \end{bmatrix}.$$

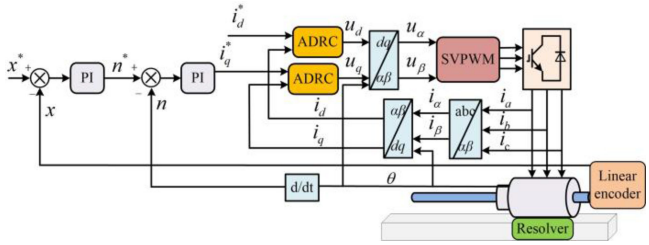

Fig. 4. Block diagram of the control structure of magnetic screw motor based on ADRC.

Combining (31) and (32), the first-order control signal x_1 and observation signals z_1 and z_2 are obtained and then the overall expression of a linear system can be expressed as

$$\begin{cases} \begin{bmatrix} \dot{\zeta}_1 \\ \dot{\zeta}_2 \end{bmatrix} = \begin{bmatrix} a_1 & -a_1 k_1 \\ 0 & -k_1 \end{bmatrix} \begin{bmatrix} \zeta_1 \\ \zeta_2 \end{bmatrix} + \begin{bmatrix} -\beta_2 \\ \beta_1 \end{bmatrix} u \\ \dot{\eta} = u \\ u = -g(y) \\ y = -\frac{\zeta_1}{a_1} + \zeta_2 - \frac{\beta_2}{a_1}\eta \end{cases} \tag{33}$$

where $\zeta_1 = a_1 x_1 - z_2$, $\zeta_2 = z_1$, $\eta = z_2/\beta_2$.

The transfer function of the abovementioned formula can be expressed as

$$f(s) = \frac{\beta_1 s^2 + (\beta_2 + k_1\beta_1 - \beta_1 a_1)\, s + k_1\beta_2}{s^3 + (k_1 - a_1)\, s^2 - a_1 k_1 s}. \tag{34}$$

According to Popov stability criterion, the condition for the absolute stability of the system must be guaranteed that $T(s) = (2l_1\rho + l_2 s)f(s)$ is a positive real function, where l_1 and l_2 are nonnegative real numbers that are not all 0. The following two conditions are satisfied at the same time: 1) $T(s)$ has at least one negative real part pole. 2) When $l_1 = 0$ with any $\varepsilon>0$, there existing $g(y) = \varepsilon y$, the system is asymptotically stable.

When l_1 is set as $1/2\rho$, $T(s)$ can be expressed as

$$T(s) = (1 + l_2 s)\frac{\beta_1 s^2 + (\beta_2 + k_1\beta_1 - \beta_1 a_1)\, s + k_1\beta_2}{s^3 + (k_1 - a_1)\, s^2 - a_1 k_1 s}. \tag{35}$$

When l_2 is set as $1/a_1$ with $a_1<0$ and $k_1>0$, $T(s)$ is a positive real function and has two negative real part poles. Therefore, the system is absolutely stable.

G. Block Diagram of the System

In this article, three closed-loop control algorithm is used to control the displacement of the magnetic screw motor. Among the current loop, speed loop, and displacement loop, ADRC is adopted to replace the traditional PI controller on the current loop. As shown in Fig. 4, the PMSM rotor is driven to rotate through space vector pulsewidth modulation. The resolver and linear encoder collect the position angle and linear displacement signals of the magnetic screw motor, respectively.

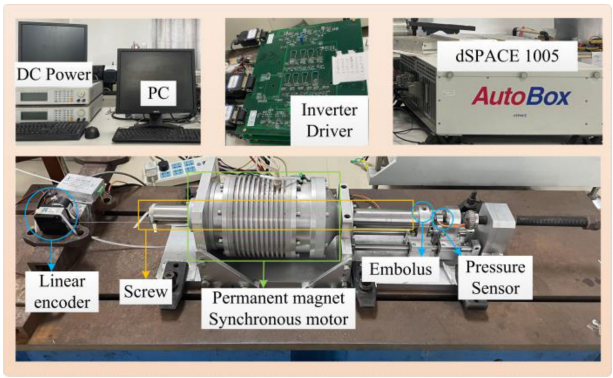

Fig. 5. Experimental platform.

TABLE I
PRACTICAL PARAMETERS

Parameters	Value
Pole pair of magnetic screw p	8
Pole-pitch of magnetic screw γ	9mm
Magnetic screw air gap radius λ	18mm
Nominal air gap length l_g	1mm
Permanent magnet thickness l_t	4mm
Mass M	8.398kg
Rated power P_N	2kW
Rated voltage U_N	380V
Rated current I_N	10A
Rated speed ω_N	2500r/min
Rated frequency f_N	233Hz
Tracking speed factor g_0	50
Parameter g_{21}	2000
Parameter g_{22}	5000
Gain g_3	2
Nonlinear factor α	0.25
error accuracy δ	0.1

IV. VERIFICATION OF EXPERIMENT

A. Experimental Platform

In order to verify the effectiveness of precise displacement of the magnetic screw linear rotating motor, an experimental platform has been established, as shown in Fig. 5. The parameters of magnetic screw and ADRC are shown in Table I.

B. Robustness Test of ADRC

The parameter b in the ADRC is related to the inductance coefficient of the motor: $b = 1/L$. The following are two sets of parameter mismatch experiments to demonstrate the robustness of ADRC. The inductance coefficient is changed to $2L$ and $1/2L$ for comparison. As shown in Fig. 6, the linear displacement can still quickly track the given signal and the current fluctuations can still be improved after the inductance coefficient changes. Therefore, the ADRC designed in this article has strong robustness.

C. Experimental Results

Fig. 7 shows the comparative experimental results of accurate linear displacement among the traditional PI control, the classical sliding mode control and the proposed ADRC. It can

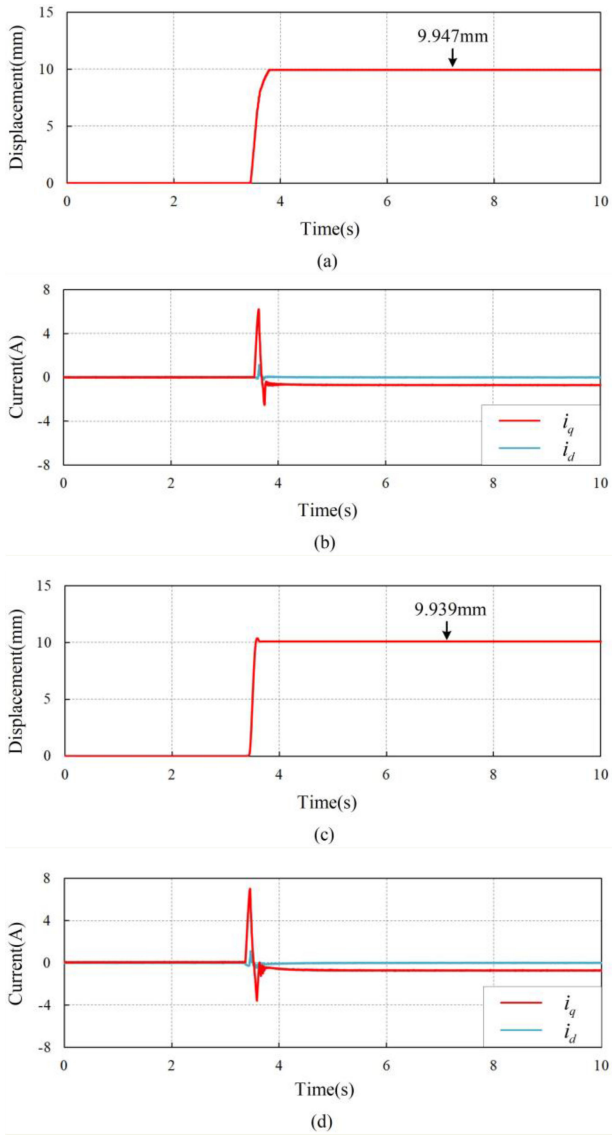

Fig. 6. (a) Linear displacement with 2L. (b) Current with 2L. (c) Linear displacement with 1/2L. (d) Current with 1/2L.

be seen that the magnetic screw motor can quickly reach the target position without overshoot, which highlights the powerful tracking effect of ADRC. Since the normal operation of the motor is greatly affected by i_q, the small fluctuation of i_q enables the motor to stabilize rapidly in a period of short time, which can be seen in Fig. 7(d). As can be seen from Fig. 7(b) and (c), the currents fluctuation under PI control and SMC are large, which deteriorates the dynamic performance of the system. Due to the inevitable existence of system lag, delay, inertia, and other factors, SMC cannot ideally reach the equilibrium point along the sliding mode surface and it will produce sawtooth jitter when passing through the sliding surface, resulting in chattering. In Fig. 7(e), although the control target can be completed, the instability of the current leads to the instability of the rotor. The previous paper explained that the closer the relative displacement is to 0, the better the control effect of the motor is. According to the formula $x_d = x + h\theta$, the relative displacement

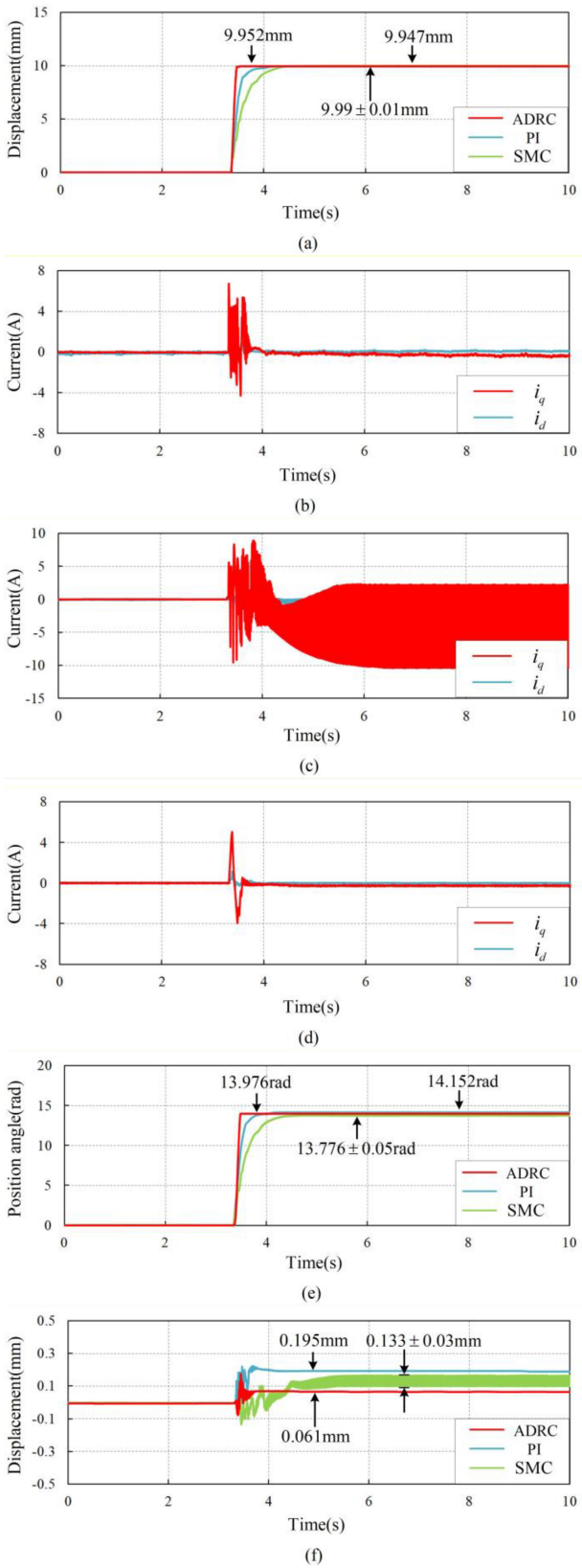

Fig. 7. Experiment with displacement of 10 mm. (a) Linear displacement. (b) Current based on PI. (c) Current based on SMC. (d) Current based on ADRC. (e) Rotor position angle. (f) Relative displacement.

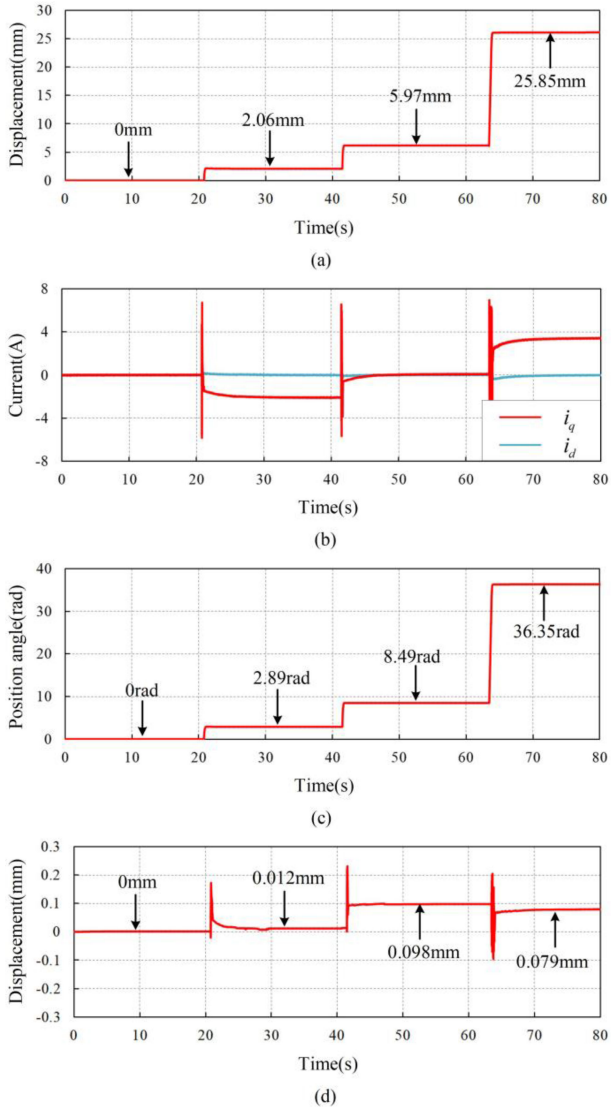

Fig. 8. Experiment of displacement mutation. (a) Linear displacement. (b) Current. (c) Rotor position angle. (d) Relative displacement.

calculated in Fig. 7(e) is affected by the linear displacement and the rotor position angle. From the equation of motion $x = -h\theta$, it can be concluded that when the motor rotor rotates clockwise, the mover will move in the opposite direction. In contrast, the relative displacement under the ADRC is smaller and the steady state can be reached quickly.

To verify the feasibility of the magnetic screw motor control experiment, a mutation experiment on the linear displacement is conducted, as shown in Fig. 8. Combining the short-distance and long-distance displacement control, the reference linear displacement is changed by 0 mm, 2 mm, 6 mm, and 26 mm at intervals of about 20 s. It can be seen from Fig. 8(a) that the linear displacement can reach the steady-state value in a short time. As shown in Fig. 8(b), the current loop reaches a steady state quickly without fluctuations under the deployment of ADRC. Then, the system maintains a small current value to keep the normal operation state of the motor. The rotor

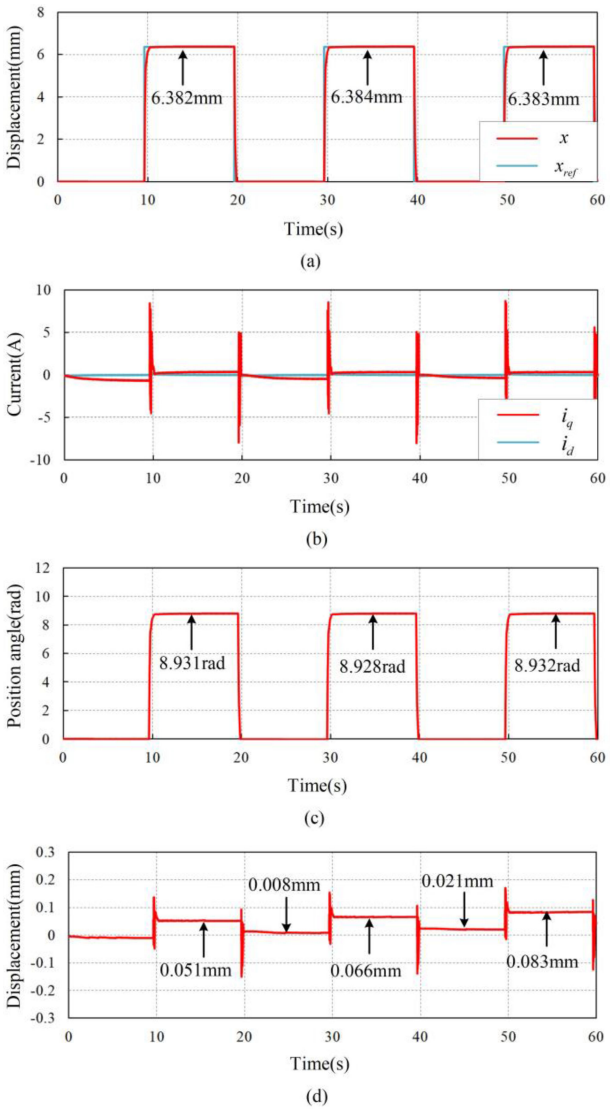

Fig. 9. Experiment of reciprocating motion controlled by step signal. (a) Linear displacement under square wave signal. (b) Current. (c) Rotor position angle. (d) Relative displacement.

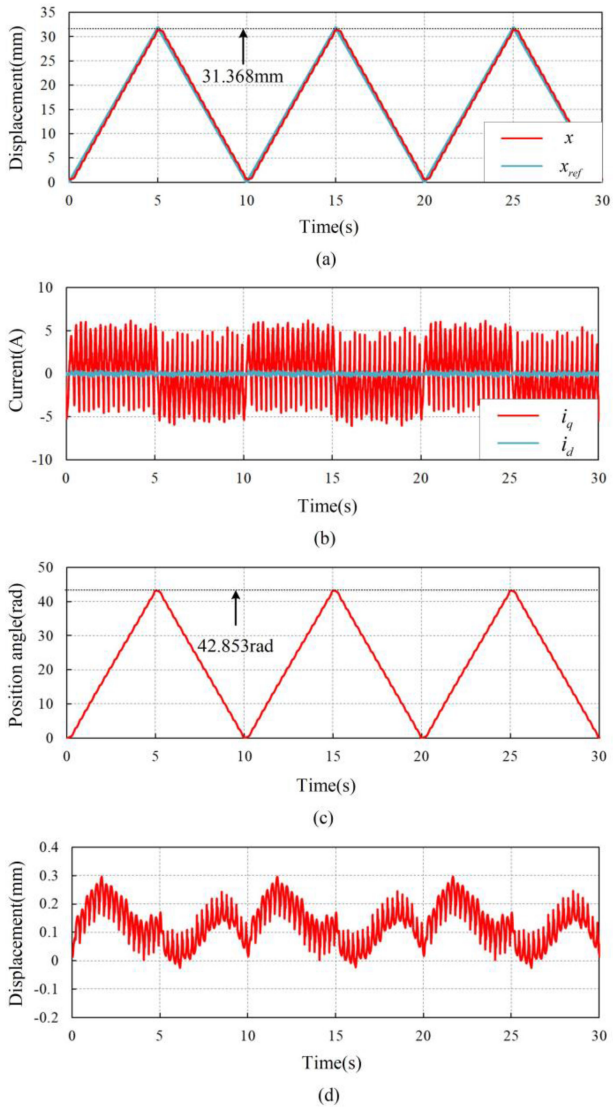

Fig. 10. Experiment of reciprocating motion controlled by ramp signal. (a) Linear displacement under triangle wave signal. (b) Current. (c) Rotor position angle. (d) Relative displacement.

position angle of the PMSM is shown in Fig. 8(c). The system undergoes three displacement mutations, and the mechanical angle changes three times simultaneously: 2.89 rad, 8.49 rad, and 36.35 rad, respectively. Through the formula $x_d = x + h\theta$, the relative displacement can be obtained, as shown in Fig. 8(d). The relative displacements are all less than 1/4λ, which indicates that the motor is working normally and the rotor does not slip. Since the position of the rotor before the initial position is unknown, the mechanical angle of rotation cannot be obtained. Therefore, the relative displacement in the first paragraph is set to 0.

Finally, the last three sets of experiments are to control the displacement of the magnetic screw motor through different input signals. The purpose is to use the reciprocating motion of the magnetic screw motor to test the tracking effect. It is worth noting that the difference from the previous experiment of displacement mutation is that there is no need to manually change the set value and the magnetic screw can always reciprocate.

As shown in Fig. 9, the input signal given in the first set of experiments is a step signal with amplitude of 6.383 mm and period of 10 s. Fig. 9(a) shows that the actual linear displacement can track the given value well. In Fig. 9(b), similar to the previous displacement mutation experiment, the current changes drastically during the movement of the magnetic screw motor and then it can stabilize after the motor reaches the given value. Combining Fig. 9(a) and (c), the relative displacement can be calculated, as shown in Fig. 9(d). The relative displacement is also very small, which shows that the magnetic screw motor has good performance under step signal control.

The next experiment is that the input signal is a triangular wave signal with peak value of 31.368 mm and period of 10 s. While the difficulty of slope signal control is that its function is not smooth, the improved ADRC just makes up for this defect. Since the input signal does not have a constant and stable given value, the magnetic screw motor is always in motion. In

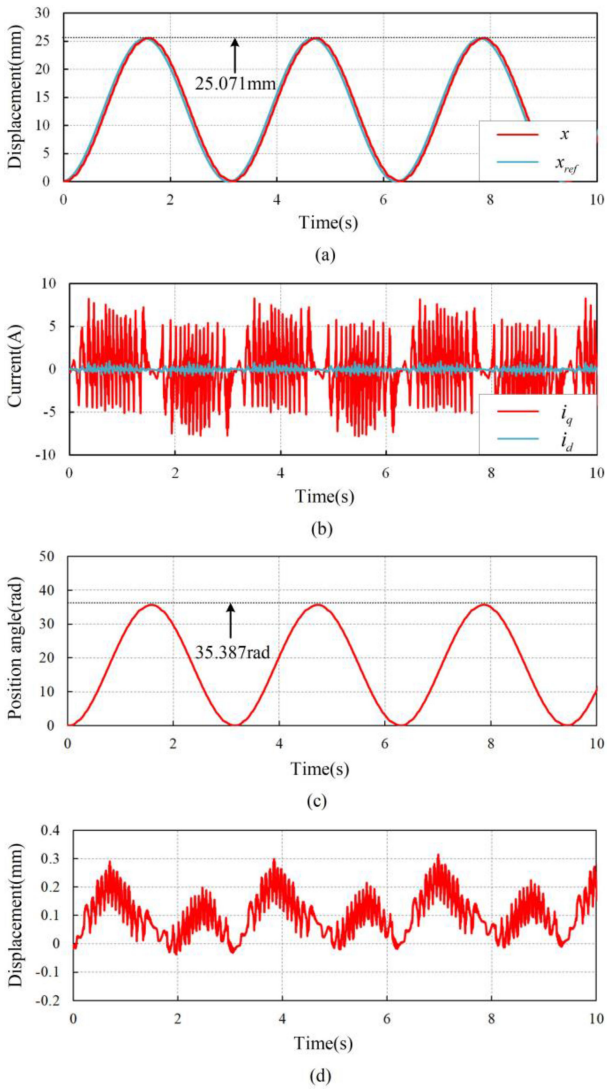

Fig. 11. Experiment of reciprocating motion controlled by sine signal. (a) Linear displacement under sinusoidal signal. (b) Current. (c) Rotor position angle. (d) Relative displacement.

Fig. 10(a), the magnetic screw motor has completed a linear displacement reciprocating motion with an average speed of about 6.274 mm/s. Fig. 10(c) depicts the *d*-axis current fluctuates around the 0 and the *q*-axis current fluctuates approximately the same amplitude. This means that the magnetic screw motor is doing approximately uniform reciprocating motion. As shown in Fig. 10(d), the small relative displacement shows the stability effect of ADRC control. Although the relative displacement is affected to some extent, the magnetic screw can still track the given signal perfectly.

The input signal of the last experiment is a sine signal with amplitude of 25.071 mm and period of 3.1 s. During this movement, the magnetic screw motor tracks the given value and completes the sinusoidal movement while the speed is changing in Fig. 11(a). As shown in Fig. 11(b), compared with ramp signal, the current fluctuation under the control of the sine signal is relatively large. When the linear displacement is near the peak or valley, the linear speed is relatively slow and the current fluctuation at this time is also relatively small. Fig. 11(c) and (d) describes the position angle of the rotor and the relative displacement.

The experiments of the precise displacement comparison under ADRC, the displacement mutation and the reciprocating motion show that the actual work of the magnetic screw motor is consistent with the theory. Furthermore, linear displacement can track the given signal in time. According to the results, the dynamic performance and anti-interference performance of the system have been effectively improved after adopting ADRC.

V. Conclusion

In this article, a novel ADRC algorithm is proposed to optimize and enrich the linear displacement of a motor composed of PMSM and magnetic screw. Compared with the traditional PI control and the classical SMC, the improved ADRC enhances the flexibility and tracking performance of the magnetic screw motor by making up for the lack of nonlinear region and reducing the current fluctuation. Finally, the dynamic performance and anti-interference ability of the system improved by ADRC are verified by rich experimental results.

References

[1] L. Xie, J. Si, Y. Hu, H. Feng, and K. Ni, "Characteristics analysis of the motions of the two-degree-of-freedom direct drive induction motor," *IEEE Trans. Ind. Electron.*, vol. 67, no. 2, pp. 931–941, Feb. 2020.

[2] C. Cheng and S. Hung, "A piezoelectric two-degree-of-freedom nanostepping motor with parallel design," *IEEE/ASME Trans. Mechatron.*, vol. 21, no. 4, pp. 2197–2199, Aug. 2016.

[3] H. Y. Kim, H. Kim, D. Gweon, and J. Jeong, "Development of a novel spherical actuator with two degrees of freedom," *IEEE/ASME Trans. Mechatron.*, vol. 20, no. 2, pp. 532–540, Apr. 2015.

[4] T. Yoshimoto, Y. Asai, K. Hirata, and T. Ota, "Dynamic characteristics of novel two-DOF resonant actuator by vector control," *IEEE Trans. Magn.*, vol. 48, no. 11, pp. 2985–2988, Nov. 2012.

[5] J. Huang, H. An, Y. Yang, C. Wu, Q. Wei, and H. Ma, "Model predictive trajectory tracking control of electro-hydraulic actuator in legged robot with multi-scale online estimator," *IEEE Access*, vol. 8, pp. 95918–95933, 2020.

[6] S. A. Evans, I. R. Smith, and J. G. Kettleborough, "Permanent-magnet linear actuator for static and reciprocating short-stroke electromechanical systems," *IEEE/ASME Trans. Mechatron.*, vol. 6, no. 1, pp. 36–42, Mar. 2001.

[7] P. Giangrande *et al.*, "Considerations on the development of an electric drive for a secondary flight control electromechanical actuator," *IEEE Trans. Ind. Appl.*, vol. 55, no. 4, pp. 3544–3554, Jul./Aug. 2019.

[8] B. Na, H. Choi, and K. Kong, "Design of a direct-driven linear actuator for a high-speed quadruped robot, Cheetaroid-I," *IEEE/ASME Trans. Mechatron.*, vol. 20, no. 2, pp. 924–933, Apr. 2015.

[9] J. Wang, G. W. Jewell, and D. Howe, "A general framework for the analysis and design of tubular linear permanent magnet machines," *IEEE Trans. Magn.*, vol. 35, no. 3, pp. 1986–2000, May 1999.

[10] J. Wang, G. W. Jewell, and D. Howe, "Design optimisation and comparison of tubular permanent magnet machine topologies," *IEE Proc. Elect. Power Appl.*, vol. 148, no. 5, pp. 456–464, Sep. 2001.

[11] J. Wang, D. Howe, and G. W. Jewell, "Analysis and design optimization of an improved axially magnetized tubular permanent magnet machine," *IEEE Trans. Energy Convers.*, vol. 19, no. 2, pp. 289–295, Jun. 2004.

[12] Z. Ling, J. Ji, J. Wang, and W. Zhao, "Design optimization and test of a radially magnetized magnetic screw with discretized PMs," *IEEE Trans. Ind. Electron.*, vol. 65, no. 9, pp. 7536–7547, Sep. 2018.

[13] M. Cirolini, A. F. Flores Filho, Y. C. Wu, and D. G. Dorrell, "Design aspects of a reluctance-based magnetic lead screw," *IEEE Trans. Magn.*, vol. 55, no. 7, Jul. 2019, Art. no. 8001906.

[14] Z. Ling, W. Zhao, P. O. Rasmussen, J. Ji, Y. Jiang, and Z. Liu, "Design and manufacture of a linear actuator based on magnetic screw transmission," *IEEE Trans. Ind. Electron.*, vol. 68, no. 2, pp. 1095–1107, Feb. 2021.

[15] Z. Liu and J. Wang, "Design and testing of a high force density linear electromagnetic actuator," in *Proc. IEEE Energy Convers. Congr. Expo.*, Oct. 2020, pp. 1145–1152.
[16] J. Ji, Z. Ling, J. Wang, W. Zhao, G. Liu, and T. Zeng, "Design and analysis of a Halbach magnetized magnetic screw for artificial heart," *IEEE Trans. Magn.*, vol. 51, no. 11, Nov. 2015, Art. no. 8108604.
[17] Z. Ling, W. Zhao, J. Ji, and G. Liu, "Design of a new magnetic screw with discretized PMs," *IEEE Trans. Appl. Superconduct.*, vol. 26, no. 4, Jun. 2016, Art. no. 0602805.
[18] F. Gao, Q. Wang, Y. Hu, B. Chen, B. Zhao, and J. Zou, "Performance evaluation of magnetic lead screws equipped with skewed arc magnets instead of helical ones," *IEEE Trans. Magn.*, vol. 54, no. 11, Nov. 2018, Art. no. 8204405.
[19] J. Wang, K. Atallah, and W. Wang, "Analysis of a magnetic screw for high force density linear electromagnetic actuators," *IEEE Trans. Magn.*, vol. 47, no. 10, pp. 4477–4480, Oct. 2011.
[20] I. A. Smadi, H. Omori, and Y. Fujimoto, "Development, analysis, and experimental realization of a direct-drive helical motor," *IEEE Trans. Ind. Electron.*, vol. 59, no. 5, pp. 2208–2216, May 2012.
[21] Y. Fujimoto, T. Kominami, and H. Hamada, "Development and analysis of a high thrust force direct-drive linear actuator," *IEEE Trans. Ind. Electron.*, vol. 56, no. 5, pp. 1383–1392, May 2009.
[22] A. Z. Shukor and Y. Fujimoto, "Direct-drive position control of a spiral motor as a monoarticular actuator," *IEEE Trans. Ind. Electron.*, vol. 61, no. 2, pp. 1063–1071, Feb. 2014.
[23] Y. Fujimoto, T. Suenaga, and M. Koyama, "Control of an interior permanent-magnet screw motor with power-saving axial-gap displacement adjustment," *IEEE Trans. Ind. Electron.*, vol. 61, no. 7, pp. 3610–3619, Jul. 2014.
[24] C. S. Cyusa and Y. Fujimoto, "Enactment-based direct-drive test of a novel radial-gap helical rotlin machine," *IEEE Trans. Ind. Appl.*, vol. 54, no. 2, pp. 1273–1282, Mar./Apr. 2018.
[25] Z. Wang, J. Zhao, L. Wang, M. Li, and Y. Hu, "Combined vector resonant and active disturbance rejection control for PMSLM current harmonic suppression," *IEEE Trans. Ind. Informat.*, vol. 16, no. 9, pp. 5691–5702, Sep. 2020.
[26] B. Du, S. Wu, S. Han, and S. Cui, "Application of linear active disturbance rejection controller for sensorless control of internal permanent-magnet synchronous motor," *IEEE Trans. Ind. Electron.*, vol. 63, no. 5, pp. 3019–3027, May 2016.
[27] W. Zhang, H. Zhu, Y. Xu, and M. Wu, "Direct control of bearingless permanent magnet slice motor based on active disturbance rejection control," *IEEE Trans. Appl. Superconduct.*, vol. 30, no. 4, Jun. 2020, Art. no. 5202205.
[28] J. Zhao, L. Wang, L. Xu, F. Dong, J. Song, and X. Yang, "Uniform demagnetization diagnosis for permanent-magnet synchronous linear motor using a sliding-mode velocity controller and an ALN-MRAS flux observer," *IEEE Trans. Ind. Electron.*, vol. 69, no. 1, pp. 890–899, Jan. 2022.

Guohai Liu (Senior Member, IEEE) received the B.Sc. degree from Jiangsu University, Zhenjiang, China, in 1985, and the M.Sc and Ph.D. degrees from Southeast University, Nanjing, China, in 1988 and 2002, respectively, all in electrical engineering and control engineering.

Since 1988, he has been with the Jiangsu University, where since 2001, he has been a Professor with the School of Electrical Information Engineering. He is currently the Director of Jiangsu Key Laboratory of Drive and Intelligent Control for Electric Vehicle. From 2003 to 2004, he was a Visiting Professor with the Department of Electronic and Electrical Engineering, University of Sheffield, Sheffield, U.K. He has authored or coauthored more than 300 technical papers and 4 textbooks, and is the holder of 60 patents in these areas. His teaching and research interests include electrical machines, motor drives for EV, and intelligent control.

Prof. Liu is a Fellow of Institution of Engineering and Technology, U.K.

Lixian Fang received the B.Sc. degree in automation in 2020 from Nanjing institute of technology, Nanjing, China, where he is currently working toward the M.Sc. degree in electronic information.

His research interests include high-performance control of electric machines and active disturbance rejection control.

Zhengmeng Liu received the B.S. degree from Chongqing University, Chongqing, China, in 2013, and the M.S. degree from Jiangsu University, Zhenjiang, China, in 2016, and the Ph.D. degree from University of Sheffield, Sheffield, U.K., in 2021, all in electrical engineering.

Since 2021, he has been with Jiangsu University, where he is currently a Lecturer with the School of Electrical Information Engineering. His research interests include the design and analysis of permanent magnet electrical machines and linear actuators.

Qian Chen (Senior Member, IEEE) received the B.Sc. and Ph.D. degrees in electrical engineering and control engineering from Jiangsu University, Zhenjiang, China, in 2009 and 2015, respectively.

Since 2015, he has been with Jiangsu University, where he is currently a Professor with the School of Electrical Information Engineering. He is a Full Member of Sigma Xi, The Scientific Research Honor Society. From 2020 to 2021, he was a Visiting Professor with the Department of Electronic and Electrical Engineering, University of Sheffield, Sheffield, U.K. His current research interests include electric machine design, modeling, fault analysis, and intelligent control.

Jiahao Zhang received the B.Sc. degree in electrical automation in 2018 from Yancheng Institute of Technology, Yancheng, China, where he is currently working toward the Ph.D. degree in control science and engineering.

His research interests include high-performance control of electric machines and position sensorless control.